MEMS, Field-Emitter, Thermal, and Fluidic Devices

Development of a Tabletop Fabrication Platform for MEMS Research, Development, and Production 85

Development of in-situ Depth Profiler for Real-Time Control in a Deep Reactive Ion Etcher.. 86

Resonant Body Transistor with MIT Virtual Source (RBT-MVS) Compact Model 87

Shielded, Flexible, and Stretchable Tactile Pressure and Shear Sensors
Based on Deformable Microwave Transmission Lines... 88

Micro-Engineered Pillar Structures for Pool-Boiling CHF Enhancement... 89

An Ultra-Thin Nanoporous Membrane Evaporator 90

Thin-Film Evaporation from Nanoporous Membranes for Thermal Management.. 91

Suppressing High-Frequency Temperature Oscillations in Microchannel Heat Sinks with Surface Structures................ 92

EWOD Actuation of a Vertical Translation and Angular Manipulation Stage 93

Additively Manufactured Miniature Diaphragm Vacuum Pumps 94

Evaluation of Lost-Wax Micromolding for Additive Manufacturing of Miniaturized Metallic Vacuum Components........ 95

3-D Printed Multiplexed Electrospinning Sources for Large Production of Nanofibers 96

Atmospheric Microplasma-Based 3-D Printing of Metallic Microstructures...97

MEMS Electrohydrodynamic High-Throughput Core-Shell Droplet Sources.. 98

High Current Density Si-field Emission Arrays (FEAs)... 99

Field Emission from Silicon Tips Embedded in a Dielectric Matrix 100

A Silicon Field Emitter Array as an Electron Source for Phase Controlled Magnetrons 101

Ion Electrospray Thrusters for Microsatellite Propulsion..102

Enhanced Water Desalination in Electromembrane Systems 103

Development of a Tabletop Fabrication Platform for MEMS Research, Development, and Production

M. D. Hsing, P. A. Gould, M. A. Schmidt
Sponsorship: MTL

A general rule of thumb for new semiconductor fabrication facilities (Fabs) is that revenues from the first year of production must match the capital cost of building the fab itself. With modern fabs routinely exceeding $1 billion to build, this rule serves as a significant barrier to entry for research and development and for groups seeking to commercialize new semiconductor devices aimed at smaller market segments and requiring a dedicated process. To eliminate this cost barrier, we are working to create a suite of tools that will process small (~1") substrates and cumulatively cost less than $1 million. This suite of tools, known colloquially as the 1" Fab, offers many advantages over traditional fabs. By shrinking the size of the substrate, we trade high die throughputs for significant capital cost savings, as well as substantial savings in material usage and energy consumption. This substantial reduction in the capital cost will drastically increase the availability of semiconductor fabrication technology and enable experimentation, prototyping, and small-scale production to occur locally and economically.

To implement this suite of 1" Fab tools, our current research has primarily been focused on developing a 1" Fab deep reactive ion etcher (DRIE). DRIE tools are used to create highly anisotropic, high aspect-ratio trenches in silicon—a crucial element in many MEMS processes that will benefit from a 1" Fab platform. In 2015-2016 we completed the development of the tool, and in this past year, our focus has been on optimizing its design for manufacturability. We ultimately demonstrated the manufacturability of the tool by setting up a satellite laboratory in Beijing, China with our research collaborators at the General Research Institute for Nonferrous Metals (GRINM). (See Figure 1 for a photo of the system set up in China). Our GRINM colleagues are helping develop etch recipes and providing feedback on the operation of the tool. We have also been working with the Perreault group at MIT to develop a low-cost, resistance-compression-based impedance matching network for use with this DRIE system and other plasma-based processing tools

In addition to the optimization of the DRIE tool, we are currently developing novel PECVD and magnetron sputtering tools. In the PECVD research, we are exploring the use of inductively coupled plasma sources and non-pyrophoric mixtures of silane gas for Si-based film depositions. For sputtering, we are looking at novel techniques for creating low cost multi-layer film stacks. These two new systems will leverage the pre-existing 1" Fab modular infrastructure and will be fully compatible with the common base assembly that was developed for the 1" Fab DRIE system, as shown in Figure 2.

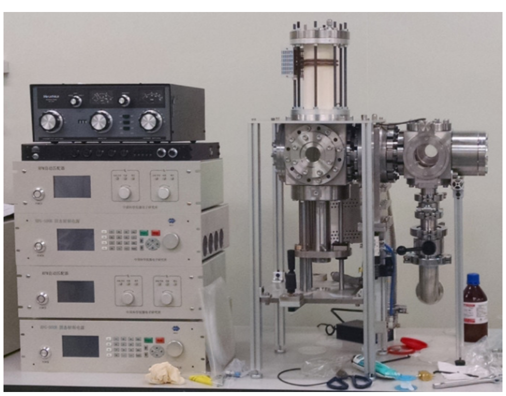

▲ Figure 1: View of the basic components of the 1" Fab DRIE system.

▲ Figure 2: 1" Fab tools utilizing a common base assembly.

FURTHER READING

- S. Heck, S. Kaza, and D. Pinner, "Creating Value in the Semiconductor Industry" [Online], available: http://www.mckinsey.com/~/media/McKinsey/dotcom/client_service/Semiconductors/PDFs/MOSC_1_Value_creation.ashx, 2011.
- P. A. Gould, M. D. Hsing, H. Q. Li, K. K. Gleason, and M. A. Schmidt, "An Ultra-Low Cost Deep Reactive Ion Etching (DRIE) Tool for Flexible, Small Volume Manufacturing," in *Solid-State Sensors, Actuators and Microsystems (TRANSDUCERS)*, 2268-2271, 2015.
- A. A. Bastami, A. Jurkov, P. A. Gould, M. D. Hsing, M. A. Schmidt, and D. J. Perreault, "Dynamic Matching System for Radio-Frequency Plasma Generation," in *IEEE Energy Conversion Congress and Exposition (ECCE)*, 1-7, 2016.

Development of in-situ Depth Profiler for Real-Time Control in a Deep Reactive Ion Etcher

C. Teale, M. A. Schmidt, G. Barbastathis

Standard process development for micro and nanofabrication etching cycles rely on open-loop trial and error testing of recipes to achieve optimal etch depths and uniformities. This strategy is non-optimal for research and fabrication of novel devices where one-of-a-kind experiments can not justify lengthy process development times. As an alternative, we are developing an in-situ depth measurement device for real-time feedback of etch depth and uniformity. This will facilitate far shorter process development times, ideally enabling the desired etch to be achieved on the first process run.

Many system constraints make this very difficult and preclude the use of existing technology. We are pursuing an optical measurement approach based on a parallelized confocal design. The measurement must be done at a distance of around 8" through an aperture of around 2" in diameter, significantly limiting the numerical aperture. We are currently investigating the fundamental resolution limits of a confocal depth measurement under these conditions. We expect the dominant noise source to be laser speckle which will result from coherent illumination of the rough surface left by the plasma etching process. Calculations and simulations indicate that the confocal depth measurement is significantly corrupted by this speckle noise, severely limiting the depth resolution to around 100 µm. The desired depth resolution is around 1 µm which should be achievable if the specke noise could be removed. By measuring and characterizing the statistical properties of the rough surface's height distribution, we hope to remove the speckle noise and significantly improve the achievable depth resolution.

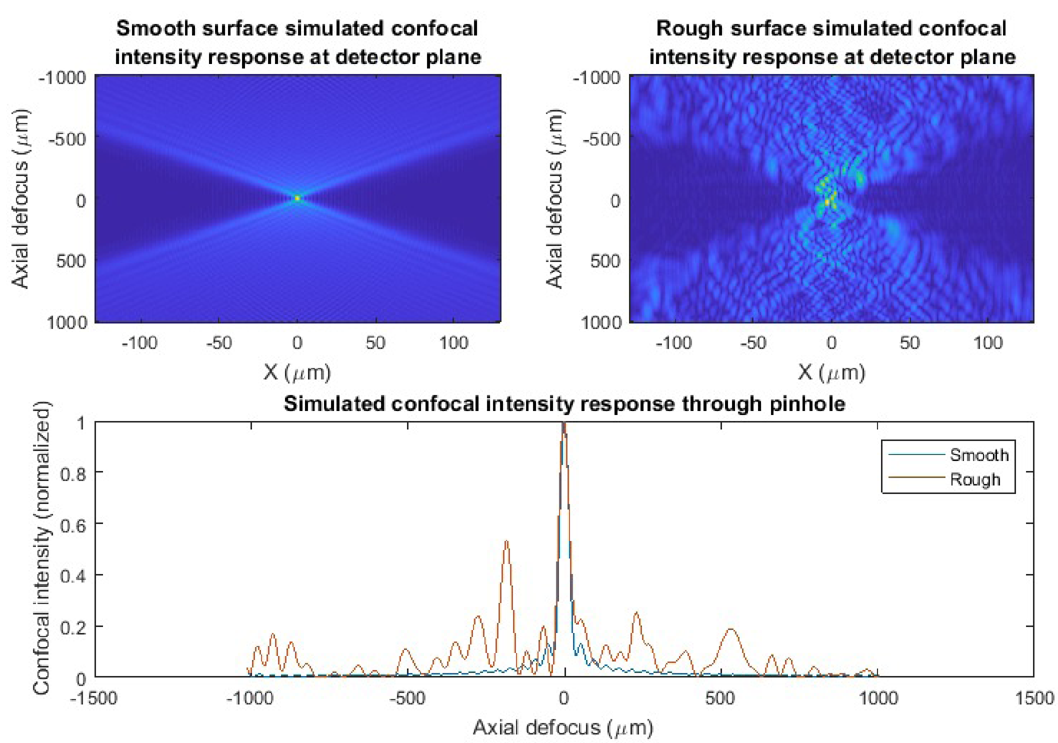

▲ Figure 1: (top, left) Smooth surface simulated confocal intensity response at detector plane, (top, right) rough surface simulated confocal instensity response at detector plane, and (bottom) simulated confocal intensity response through pinhole.

FURTHER READING

- Cha, Sungdo, et al., "Nontranslational Three-Dimensional Profilometry by Chromatic Confocal Microscopy with Dynamically Configurable Micromirror Scanning." *Applied optics* 39.16: 2605-2613, 2000.
- J. W. Goodman, "Some Fundamental Properties of Speckle," *J. Opt. Soc. Am.* 66, 1145-1150, 1976.

Resonant Body Transistor with MIT Virtual Source (RBT-MVS) Compact Model

B. Bahr, D. Weinstein, L. Daniel
Sponsorship: NSF NEEDS

High-Q mechanical resonators are crucial components for filters and oscillators that are essential for radio frequency and analog circuits. It is highly desirable for resonators to scale to GHz-frequencies and beyond to meet today's challenging requirements in terms of speed and data rates. Furthermore, aggressive scaling requirements call for monolithic integration with complementary metal-oxide semiconductor (CMOS) circuits to allow for a smaller footprint and reduced parasitics and power consumption. Micro-electro-mechanical (MEM) resonators represent a potential solution for frequency and footprint scaling, along with monolithic integration in CMOS.

A resonant body transistor (RBT) is a MEM resonator with a field-effect transistor (FET) incorporated into the resonator structure. The FET is intended for active sensing of the mechanical vibrations through piezoresistive modulation of the channel mobility. RBTs also rely on electrostatic internal dielectric transduction for actuation, by means of metal–oxide–semiconductor capacitors (MOSCAPs). Such sensing and actuation enable these devices to easily scale to multi-GHz frequencies while being compatible with CMOS manufacturing technologies.

Compact modeling for these devices is essential to gain a deeper insight into the tightly coupled physics of the RBT while emphasizing the effect of the different parameters on the device performance. It also grants circuit designers and system architects the ability to quickly assess the performance of prospective RBTs while minimizing the need for computationally intensive coupled-multiphysics finite element method (FEM) simulations.

The RBT compact model is developed as a set of modules, each representing a physical phenomenon. Mechanical resonance, FET sensing, MOSCAP driving, and thermal modules are the most notable. The modules are interconnected through a set of nodes (namely, mechanical nodes and a thermal node) to represent the coupling between the different physics. This modular approach enables the seamless expansion of the RBT model either by incorporating new physics, adding driving or thermal sources, or mechanically coupling multiple RBTs together. A modified version of the MIT Virtual Source (MVS) model is used to implement both the electrostatic driving (as a MOSCAP) and the piezoresistive active FET sensing. The full model is developed in Verilog-A and available on nanohub.org.

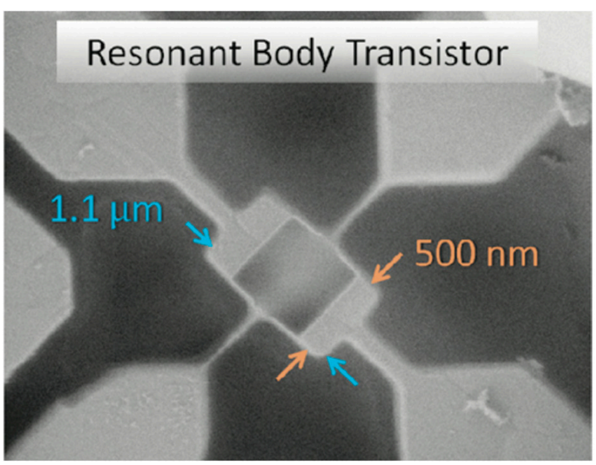

▲ Figure 1: The first RBT, developed by D. Weinstein and S. Bhave in 2009 at Cornell University.

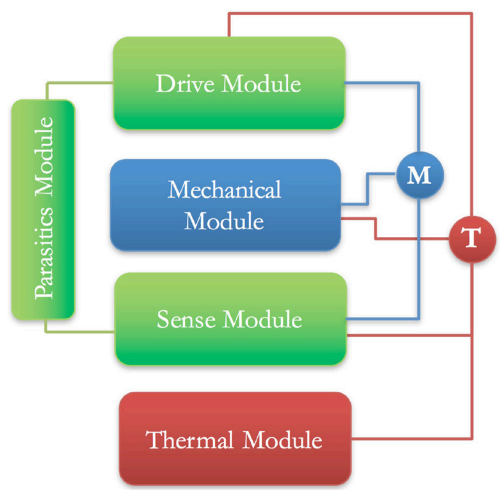

▲ Figure 2: Modular RBT model, with each physical phenomenon represented by a module. Different modules are connected through a mechanical node (M) and thermal node (T).

FURTHER READING

- D. Weinstein and S. Bhave, "The Resonant Body Transistor," *Nano Lett.*, 1234–1237, 2010.
- B. Bahr, D. Weinstein, and L. Daniel, "RBT-MVS model," nanohub.org, [Online]. Available: https://nanohub.org/publications/72/1
- B. Bahr, D. Weinstein, and L. Daniel, "URBT-MVS model," nanohub.org. [Online]. Available: https://nanohub.org/publications/132/1

Shielded, Flexible, and Stretchable Tactile Pressure and Shear Sensors Based on Deformable Microwave Transmission Lines

M. E. D'Asaro, D. B. Sheen, J. H. Lang
Sponsorship: NSF CSNE

Tactile sensors and skins aimed at replicating the human sense of touch are an active topic of research with numerous potential applications in areas including robotics, healthcare, and prosthetics. Current skin technology is limited by mechanical fragility, complex fabrication, and the need for large numbers of connections to external electronics. We have developed a new sensing technology based on microwave transmission lines that address these challenges.

The pressure sensor (Figure 1) consists of a shielded flexible and stretchable 3-mm-thick transmission line constructed with conductors made of stretchable conductive cloth and a dielectric made of silicone rubber. Where pressure is applied, the dielectric deforms causing a change in the local characteristic impedance of the line. We have developed an algorithm that can reconstruct the deformation of the line as a function of position, based on the terminal impedance of the line measured across a wide frequency range (30 MHz to 6 GHz). This algorithm can also correct for resistive loss in the transmission line. To demonstrate this sensor, three different pressure deformations were applied at each of three locations, and the responses were combined to create Figure 1. Due to the shielding, the sensor performs correctly even when tied in a knot (with updated baseline subtraction).

We have also developed a shear sensor (Figure 2) capable of measuring deformation due to applied pressure, and separately, deformation due to the force applied parallel to the surface of the sensor. This device consists of two independent transmission lines, which are constructed so that pressure causes equal impedance change but shear causes unequal change, allowing pressure to be differentiated from shear. Shear sensors are rare in the field of tactile skins; this technique, requiring only two connections, has promise for inexpensive and simple wide-area flexible and stretchable pressure and shear sensors.

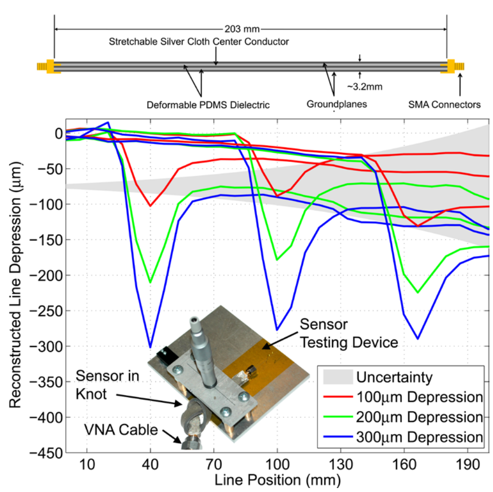

▲ Figure 1, top: Diagram of shielded pressure sensor. Main: Loss-corrected response of sensor to pressure of various magnitudes and at various locations. Inset: Sensor on testing apparatus shown tied in a knot with no significant effect on response.

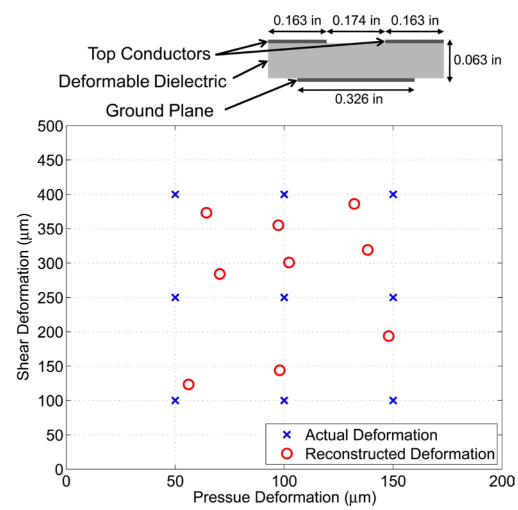

▲ Figure 2, top: Cross-section of shear sensor showing conductors and dielectric. Main: Sensor response to various magnitudes of simultaneous pressure and shear. (Actual applied pressure and shear plotted for comparison.)

FURTHER READING

- M. E. D'Asaro, D. B. Sheen, and J. H. Lang, "Thin Flexible and Stretchable Tactile Sensor Based on a Deformable Microwave Transmission Line," *Hilton Head 2016 Workshop on Solid-State Sensors, Actuators and Microsystems*, 278-281, Jun. 2016.
- M. E. D'Asaro, D. B. Sheen, and J. H. Lang, "A Fully-Shielded Flexible and Stretchable Microwave Transmission-Line Tactile Pressure Sensor," *2016 IEEE Sensors*, 1-3, Oct. 2016.
- M. E. D'Asaro, "Flexible and Stretchable Tactile Sensing Skins using Microwave Transmission Lines and Piezoresistive Rubber," Ph.D. Thesis, Massachusetts Institute of Technology, Cambridge, MA, 2017.

Micro-Engineered Pillar Structures for Pool-Boiling CHF Enhancement

M. Rahman, G. Saccone, M. Bucci, J. Buongiorno
Sponsorship: Exelon Corporation, MISTI

Increasing the performance of phase-change heat transfer phenomena is key to the development of next-generation electronics as well as power generation systems and chemical processing components. Surface-engineering techniques could be successfully deployed to achieve this goal. For instance, by engineering micro/nano-scale features, such as pillars, on the boiling surface, it is possible to attain 100% enhancement in pool boiling critical heat flux (CHF). Researchers have been working on several CHF enhancing micro- and nano-structured surfaces for years. However, due to the complexity of CHF phenomena, there is still no general agreement on the enhancement mechanism. An investigation of the effect of micropillar height on surface capillary wicking and the associated pool-boiling CHF enhancement has been conducted. Several silicon micropillar structures have been fabricated using MTL photolithography and DRIE facilities.

The surfaces were characterized using MTL's scanning electron microscope (SEM), as shown in Figure 1a. The surfaces were then characterized by measuring the capillary wicking rate as presented in Figure 1b. A mechanistic capillary wicking estimation has been provided and compared with experimental wicking results (Figure 1c). Finally, the performance of such structures was characterized through traditional pool boiling experiments (Figure 1d). The results demonstrate the benefits of wicking promoted by these structures in terms of CHF enhancement.

The microstructured surfaces fabricated at MTL have also been tested in pool-boiling with an electric field applied to replace for low gravity in space applications. A further increase in CHF has been observed due to the application of the electric field, on both flat and micro-structured silicon heaters. Notably, the combined use of passive (micro-structured surfaces) and active (electric field) CHF enhancement techniques has produced the maximum CHF enhancement.

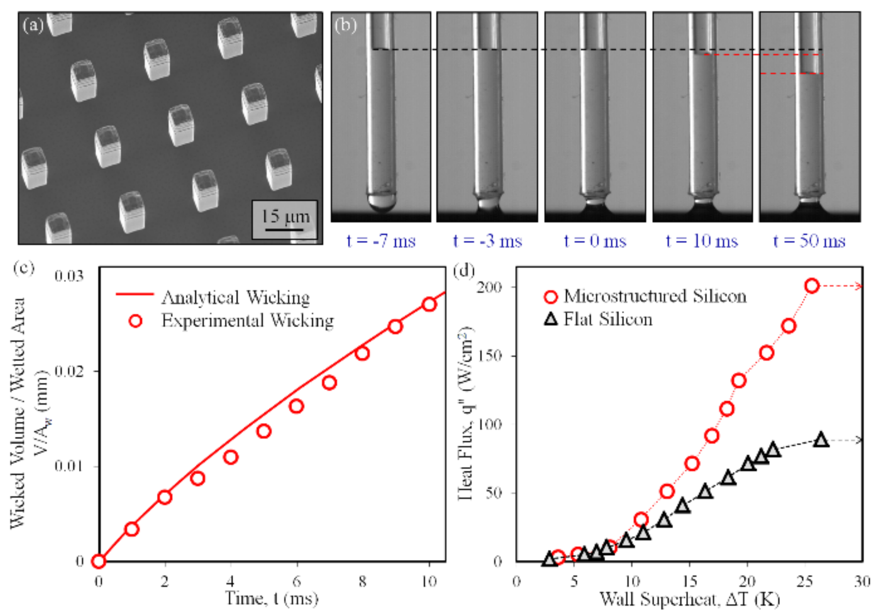

▲ Figure 1: Microstructured surfaces for CHF enhancement, (a) SEM image of a fabricated surface, (b) high speed images wicking experiment, (c) comparison of analytical and experimental wicking, (d) pool boiling result of a microstructured surface compared to flat silicon reference surface.

An Ultra-Thin Nanoporous Membrane Evaporator

Z. Lu, K. L. Wilke, D. J. Preston, I. Kinefuchi, E. Chang-Davidson, E. N. Wang
Sponsorship: AFOSR

Evaporation is a ubiquitous phenomenon found in nature and widely used in industry. Fundamental understanding of the interfacial transport during evaporation remains limited to date as it is generally challenging to characterize the heat/mass transfer at the interface level, especially when the heat flux is high (> 100 W/cm2). In this work, we were able to accurately monitor the temperature of the liquid-vapor interface, reduce the thermal-fluidic transport resistance, and mitigate the clogging risk due to contamination. This was done with an ultra-thin (≈ 200-nm thickness) nanoporous (≈ 130-nm pore diameter) membrane evaporator, Figure 1 a, b, and c. At a steady state, we demonstrated high heat fluxes across the interface (≈ 500 W/cm2) with pure evaporation into an air ambient over a total evaporation area of 0.20 mm2. In the high flux regime, we showed the breakdown of Fick's first law of diffusion and the importance of convective transport caused by evaporation itself (Figure 2). The present work improves the fundamental understanding of evaporation and paves the way for applications of high flux phase change devices.

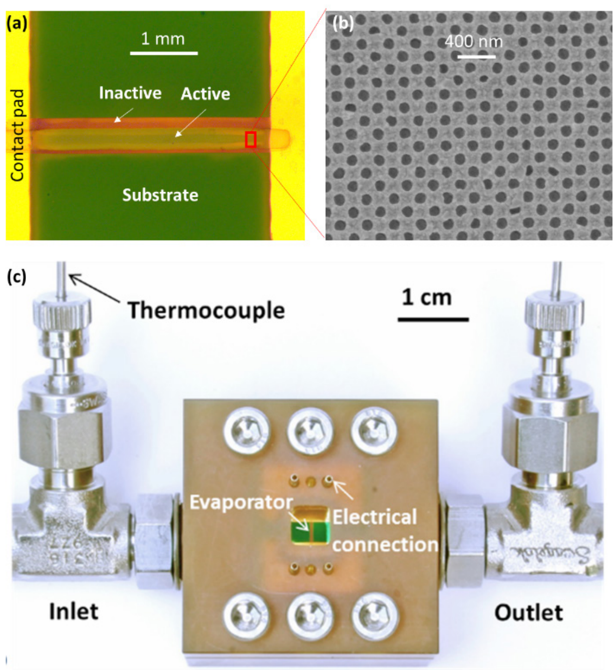

▲Figure 1: (a) Image of the ultra-thin nanoporous evaporator from an optical microscope: two Au contact pads are connected by a suspended membrane (~ 200-nm thick); the active part is nanoporous and coated with Au (≈ 40-nm thick) while the inactive part is impermeable and non-metallic, (b) image of the nanopores patterned in the active part of the membrane from a scanning electron microscope, (c) image of the test rig with a liquid feed-through and electrical connections.

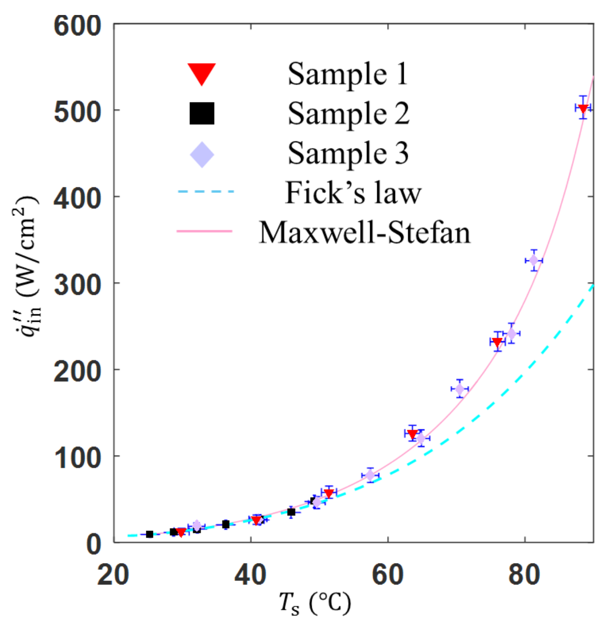

▲Figure 2: Heat flux $\dot{q}''_{in}$ vs. surface temperature T_s over a large range of evaporative heat fluxes: the red triangles, black squares, and purple diamonds are the experimental data from Samples 1, 2, and 3, respectively. The blue dash line and the pink solid line represent the model prediction from Fick's law and the Maxwell-Stefan equation, respectively.

Thin-Film Evaporation from Nanoporous Membranes for Thermal Management

K. L. Wilke, B. Barabadi, Z. Lu, T. J. Zhang, E. N. Wang
Sponsorship: The Masdar Institute of Science and Technology, MIT

Performance and lifetime of emerging electronics are often dictated by the ability to dissipate heat generated in the device. In fact, a number of advanced electronics can generate heat fluxes exceeding 1000 W/cm2, such as gallium nitride high electron mobility transistors, and pump lasers. To put that in context, the heat flux of a typical electric stovetop is more than 100x less. The large heat fluxes generated in these devices, coupled with the negative impact on the device's performance, has created the need for new thermal management techniques. Thin-film evaporation from nanopores has emerged as a promising candidate by reducing the thermal transport resistance across the liquid film while simultaneously providing capillary pumping. The combination of low resistance and large capillary pumping allows large heat fluxes to be dissipated with minimal temperature rise in the device.

In this work, we study the dependence of evaporation from nanopores on a variety of geometric parameters, including pore diameter, membrane porosity, and the location of the meniscus within the pore. Anodic aluminum oxide membranes were used as an experimental template. A bi-philic treatment was used to create a hydrophobic section of the pore to control meniscus location. This membrane was sealed in a text fixture shown in Figure 1. Heat was supplied to the membrane, and the resulting temperature was monitored.

We demonstrated different heat transfer regimes and observed more than an order-of-magnitude increase in dissipated heat flux by confining fluid within the nanopore, as seen in Figure 2. Similar tests were run systematically varying pore diameter, porosity, and meniscus location within the pore. We were able to show that pore diameter had little effect on evaporation performance at these pore diameters due to the negligible conduction resistance from the pore wall to the evaporating interface. The dissipated heat flux scaled linearly with porosity as the evaporative area increased. Furthermore, it was demonstrated that moving the meniscus as little as 1 μm into the pore could decrease performance significantly. The results of this study provide a better understanding of evaporation from nanopores and provide guidance in future high heat flux thermal management device design.

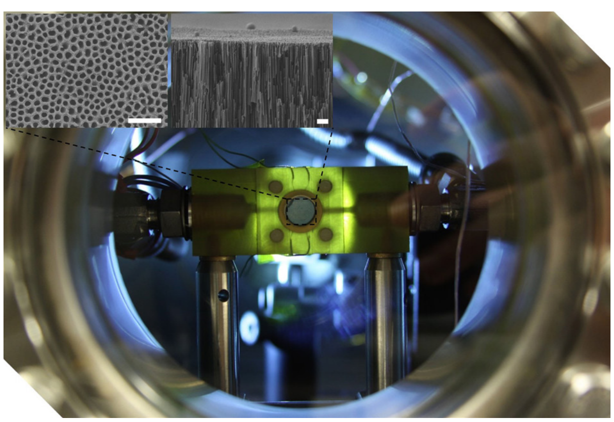

▲ Figure 1: Test fixture seen from a viewport in the experimental vacuum chamber. Insets show scanning electron microscopic images of the anodic aluminum oxide membranes used for evaporation tests. Scale bars: 1μm

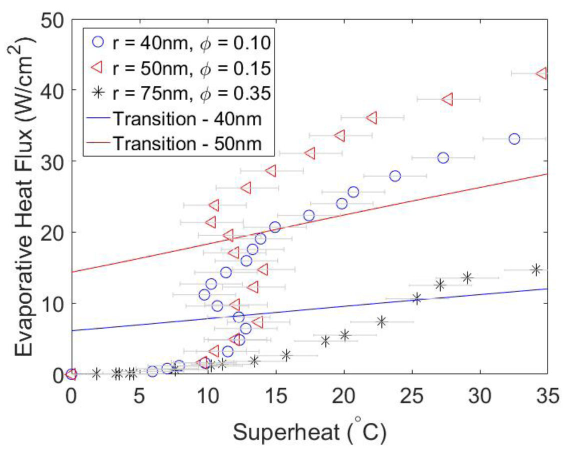

▲ Figure 2: Surface temperature vs. heating power for samples of different pore diameter and porosity.

FURTHER READING

- K. L. Wilke, B. Barabadi, T. J. Zhang, E. N. Wang, "Controlled Wetting in Nanoporous Membranes for Thin Film Evaporation," *J. Heat Transfer*, vol. 138, no. 8, 080906, 2016.
- K. L. Wilke, "Evaporation from Nanoporous Membranes," Master's Thesis, Cambridge: Massachusetts Institute of Technology, http://hdl.handle.net/1721.1/104571, 2016.

Suppressing High-Frequency Temperature Oscillations in Microchannel Heat Sinks with Surface Structures

Y. Zhu, D. S. Antao, J. D. Sircar, T. J. Zhang, E. N. Wang
Sponsorship: ONR

Thermal management of high performance electronic devices such as gallium nitride (GaN) power amplifiers and solid-state lasers is critical for their efficient and reliable operation. Two-phase microchannel heat sinks are attractive for thermal management of high heat flux electronic devices, yet flow instability, which can lead to thermal and mechanical fatigue, remains a significant challenge. Much work has focused on long-timescale (~seconds) flow oscillations, which are usually related to the compressible volume in the loop. However, the rapid growth of vapor bubbles, which can also cause flow reversal, occurs on a much shorter timescale (~tens of milliseconds). While this high-frequency oscillation has often been visualized with high-speed imaging, its effect on the instantaneous temperature has not been fully investigated due to the typical low sampling rates of the sensors.

We propose to suppress this high-frequency temperature oscillation using surface microstructures that promote capillary wicking during flow boiling. We fabricated microchannels with micropillar arrays on the bottom heated surface (Figure 1). The geometries of the micropillars were optimized based our previously developed numerical model that maximizes the capillary flow. We then investigate the temperature response as a result of the high-frequency flow oscillation in microchannel heat sinks with smooth and microstructured surfaces with a measurement data acquisition rate of 1000 Hz. For smooth surface microchannels, the fluid flow oscillated between a complete dry-out and a rewetting annular flow due to the short-timescale flow instability, which caused high-frequency and large amplitude temperature oscillations (10 ˚C in 25 ms, Figure 2a). In comparison, hydrophilic surface structures on the microchannel promoted capillary flow, which delayed and suppressed dry-out in each oscillation cycle, and thus significantly reduced the temperature oscillation (Figure 2b) at high heat fluxes. This work suggests that promoting capillary wicking via surface structures is a promising technique to reduce thermal fatigue in high heat flux, two-phase, microchannel thermal management devices.

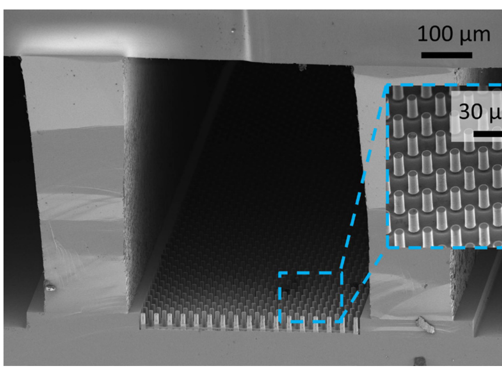

▲ Figure 1: Scanning electron micrograph of the cross-sectional view fabricated microchannel (width = height = 500 μm) with microstructures investigated in this study. Magnified view shows the micropillar arrays (diameter d=10 μm, pitch l=30 μm, and height h=25 μm).

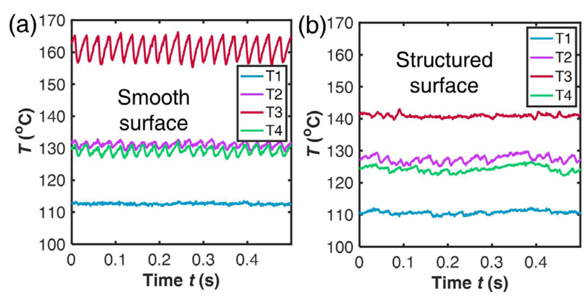

▲ Figure 2: Time-resolved temperature measurement of (a) a smooth surface microchannel and (b) a structured surface microchannel (mass flux = 100 kg/m^{2}s, heat flux = 400 W/cm^2). T1-T4 are the measured temperatures along various locations at the backside of the microchannel.

FURTHER READING

- Y. Zhu, D. S. Antao, Z. Lu, S. Somasundaram, T. J. Zhang, and E. N. Wang, "Prediction and Characterization of the Dry-out Heat Flux from Micropillar Wick Structures," *Langmuir*, vol. 32, 1920-1927, 2016.
- Y. Zhu, D. S. Antao, D. W. Bian, S. R. Rao, J. D. Sircar, T. J. Zhang, and E. N. Wang, "Suppressing High-Frequency Temperature Oscillations in Microchannels with Surface Structures," *Applied Physics Lett.*, vol. 110, 033501, 2017.
- Y. Zhu, D. S. Antao, K.-H. Chu, S. Chen, T. J. Hendricks, T. J. Zhang, and E. N. Wang, "Surface Structure Enhanced Microchannel Flow Boiling," *J. Heat Transfer*, vol. 138, 091501, 2016.

EWOD Actuation of a Vertical Translation and Angular Manipulation Stage

D. J. Preston, A. Anders, B. Barabadi, E. Tio, Y. Zhu, D. A. Dai, E. N. Wang
Sponsorship: ONR

Adhesion and friction during physical contact of solid components in microelectromechanical systems (MEMS) often lead to device failure. Translational stages that are fabricated with traditional silicon MEMS typically face these tribological concerns. Meanwhile, electrowetting, a phenomenon whereby the contact angle of a fluid can be changed with an applied voltage, allowing control of droplet shape, has had a limited role in MEMS applications. We show through modeling and experimental demonstration that the electrowetting-on-dielectric (EWOD) technique has the potential to eliminate solid-solid contact during MEMS stage operation by actuating via deformable liquid droplets placed between the stage and base to achieve stage displacement as a function of applied voltage (Figure 1).

Our EWOD stage is capable of linear spatial manipulation with resolution of 10 μm over a maximum range of 130 μm and angular deflection of approximately ±1°, comparable to piezoelectric actuators (Figure 2). We demonstrate with our model that a higher intrinsic contact angle on the EWOD surface can further improve the translational range, which was validated experimentally by comparing different surface coatings. The capability to operate the stage without solid-solid contact offers potential improvements for applications in micro-optics, actuators, and other MEMS devices.

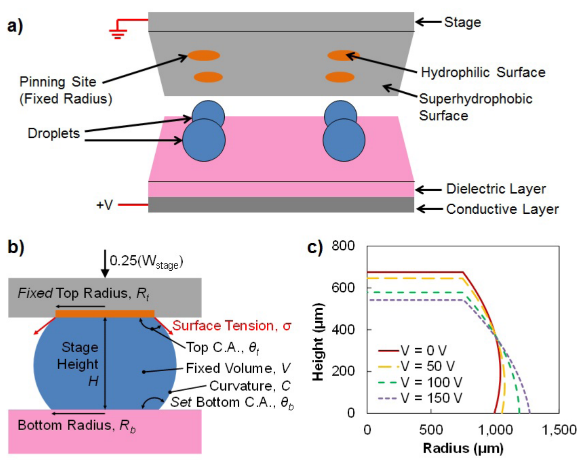

▲Figure 1: (a) Tops of the droplets contact the underside of the stage at hydrophilic copper pinning sites surrounded by a superhydrophobic surface, and bottoms of the droplets rest on the EWOD-actuated base, (b & c) device actuation is modeled for a single axisymmetric droplet, with expected stage height shown for a 2-μL droplet on a surface with a Young contact angle of 110°.

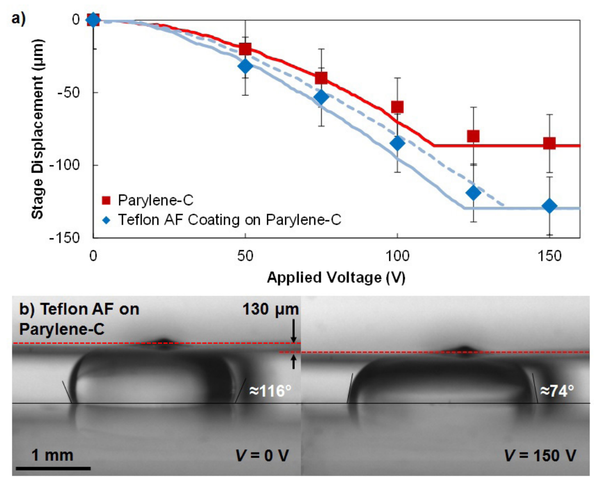

▲Figure 2: (a) Combining the Lippmann-Young equation with the axisymmetric droplet model shown in Figure 1 b & c allows prediction of the stage height as a function of applied voltage, which is in good agreement with the experimental results for stage deflection, (b) experimental images show the stage vertical translation at an applied voltage of 150 V, which resulted in a deflection of 130 μm.

FURTHER READING

- D. J. Preston, A. Anders, B. Barabadi, E. Tio, Y. Zhu, D. A. Dai, and E. N. Wang, "Electrowetting-on-Dielectric Actuation of a Vertical Translation and Angular Manipulation Stage," *Applied Physics Lett.*, vol. 109, no. 24, 244102, 2016.
- A. Cavalli, D. J. Preston, E. Tio, D. W. Martin, N. Miljkovic, E. N. Wang, F. Blanchette, and J. W. M. Bush, "Electrically Induced Drop Detachment and Ejection," *Physics of Fluids*, vol. 28, no. 2, 022101, 2016.
- H. Wang, J. T. Gaskins, C. R. Knospe, and M. L. Reed, "The Capillary Force Actuator: Design, Fabrication and Characterization," in *Proc. IEEE MEMS Conference*, 185-1188, 2012.

Additively Manufactured Miniature Diaphragm Vacuum Pumps

A. P. Taylor, L. F. Velásquez-García
Sponsorship: Edwards Vacuum

Miniaturized pumps supply fluids at precise flow rates and pressure levels in a wide variety of microfluidic systems. In particular, microfabricated positive displacement pumps that exploit gas compressibility to create vacuum have been reported as a first pumping stage in non-zero flow, reduced-pressure miniaturized systems, such as mass spectrometers. Compared to standard microfabrication, additive manufacturing offers the advantages of rapid prototyping, larger displacements for better vacuum generation and larger flow rate, freeform geometries, and a broader material selection while attaining minimum feature sizes on par with microfluidic systems (out-of-plane features in the 10-300-µm range and in-plane features in the 25-500-µm range). In addition, a number of 3-D printing techniques make possible the definition of leak-tight, closed channels or cavities, sometimes involving a second sacrificial material that is removed after printing.

Using polyjet 3-D printing technology with 42-µm XY pixelation and 25-µm layer height, a single-stage vacuum pump design with active valves and a total pumping volume of 1 cm^3 with 5% dead volume was implemented (Figure 1a). Devices were printed in the acrylate based, UV curable photopolymer TangoBlack Plus® (Shore 27A) in one piece (Figure 1b) or in two halves for ease in removing the sacrificial material. The pumps were pneumatically actuated and consistently pumped down a 1 cm^3 volume from atmosphere to 330 Torr in under 50 seconds operating at 3.27 Hz (Figure 2); from the data, the effective flow rate of the device is estimated at 8.7 cm^3/min.

The compression chamber diaphragms exhibited lifetimes approaching 20,000 cycles, while the valves' membranes have not leaked after >1-million cycles. Current work focuses on increasing the diaphragm lifetime, reducing the ultimate pressure, and improving the mass flow rate vs. pressure pump characteristics.

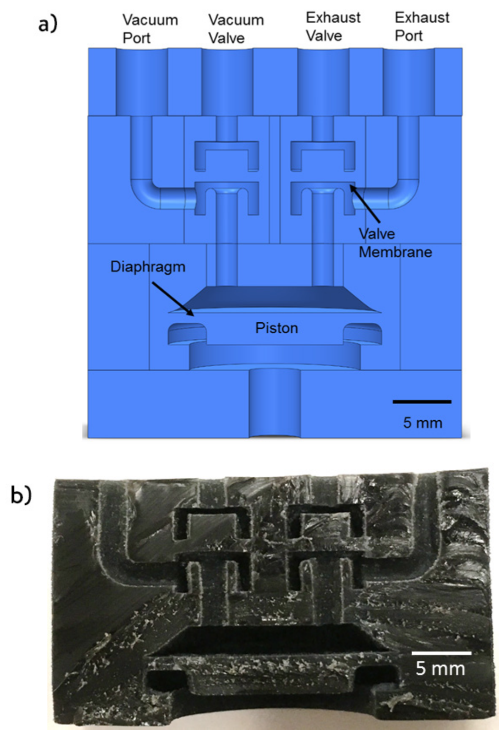

▲ Figure 1: (a) Design of the miniature diaphragm pump, and (b) image of a pump printed in one piece.

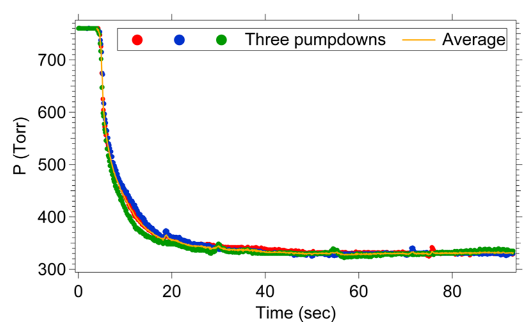

▲ Figure 2: Vacuum port pressure vs. time for several pump downs and average pump down characteristic, 3.27 Hz actuation.

FURTHER READING

- L. F. Velásquez-García, "SLA 3-D-Printed Arrays of Miniaturized, Internally-Fed, Polymer Electrospray Emitters," *J. Microelectromechanical Systems*, vol. 24, no. 6, 2117-2127, 2015.
- D. Olvera-Trejo and L. F. Velásquez-García, "Additively Manufactured MEMS Multiplexed Coaxial Electrospray Sources for High-Throughput, Uniform Generation of Core-Shell Microparticles," *Lab Chip*, vol. 16, no. 21, 4121-4132, 2016.
- A. P. Taylor and L. F. Velásquez-García, "3-D Printed Miniaturized Diaphragm Vacuum Pump," *Technical Digest 30th IEEE Conference on Micro Electro Mechanical Systems (MEMS 2017)*, 1292-1295, Jan. 2017.

Evaluation of Lost-Wax Micromolding for Additive Manufacturing of Miniaturized Metallic Vacuum Components

Z. Sun, L. F. Velásquez-García
Sponsorship: MIT, Skoltech Program

In contrast to traditional subtractive methods, additive manufacturing (AM) is a process of joining materials layer by layer to generate solid structures from computer-aided design (CAD) data. Benefits of AM include the reduction of the raw materials required to make the part, fast manufacturing speed, versatility, and adaptability. Furthermore, AM has the potential to enable novel designs that could not be fabricated with conventional machining practices and to enhance the capability of true 3-D micromanufacturing. Standard 3-D printing of metallic parts is done via selective laser sintering, where a coherent photon beam is used to create a solid from the melting of metal powders. However, the printed structures are coarse and porous with profusely outgassing surfaces and have electrical conductivity and mechanical strength less than those of the bulk material. Therefore, there is a need for better AM technologies to fabricate vacuum-compatible miniaturized metallic structures.

In this project, we are exploring lost-wax micromolding as an alternative AM technology for metal parts. Wax masters printed via stereolithography were duplicated in sterling silver by encasing the master in a ceramic mold, removing the wax by melting it, and filling-in with metal the cavities left within the mold after wax removal; finally, the parts are extracted from the mold and polished. An array of pillars (Figure 1) with diameter varying from 350 µm to 500 µm and height from 400 µm to 950 µm was created to characterize feature size repeatability (Figure 2). We found close agreement between the intended and cast heights for cylinders 400 µm to 750 µm tall; however for taller cylinders, the measured values are smaller than expected, and the standard deviation is also larger. This might be related to the way high aspect-ratio pillars with a small diameter solidify during casting. Further work will focus on completing the exploration of this technology to print solid, pore-free metal parts including characterization of physical properties such as roughness, thermal diffusivity, and vacuum outgassing.

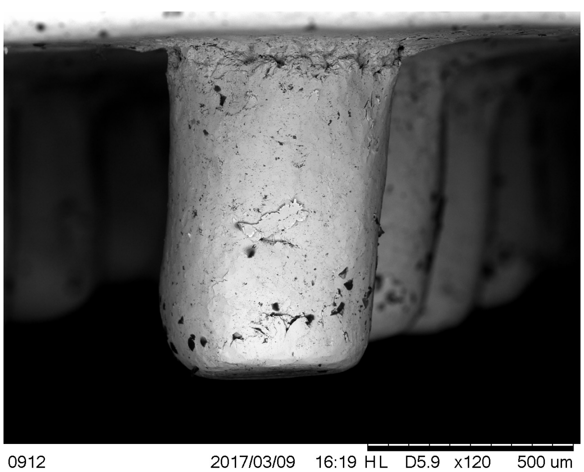

▲ Figure 1: Scanning electron microscope (SEM) image of the side view of one pillar in the sterling silver resolution matrix.

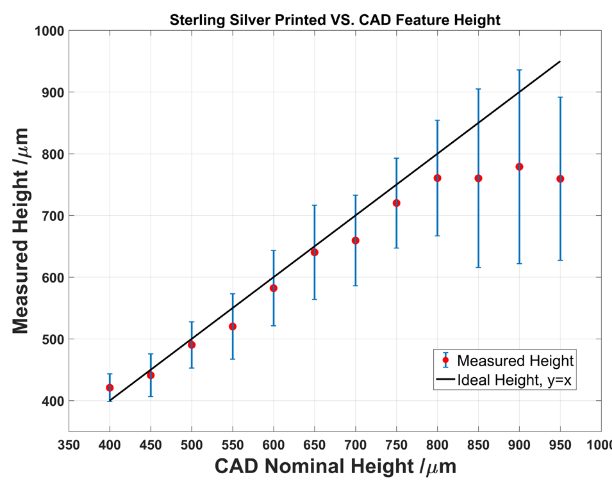

▲ Figure 2: Measured lost-wax cast height vs. CAD file height in the sterling silver resolution matrix.

FURTHER READING

- L. F. Velásquez-García, "SLA 3-D-Printed Arrays of Miniaturized, Internally-Fed, Polymer Electrospray Emitters," *J. Microelectromechanical Systems*, vol. 24, no. 6, 2117 – 2127, 2015.
- D. Olvera-Trejo and L. F. Velásquez-García, "Additively Manufactured MEMS Multiplexed Coaxial Electrospray Sources for High-Throughput, Uniform Generation of Core-Shell Microparticles," *Lab Chip*, vol. 16, no. 21, 4121 – 4132, 2016.
- A. P. Taylor and L. F. Velásquez-García, "3-D Printed Miniaturized Diaphragm Vacuum Pump," *Technical Digest 30th IEEE Conference on Micro Electro Mechanical Systems (MEMS 2017)*, 1292 – 1295, Jan. 2017.

3-D Printed Multiplexed Electrospinning Sources for Large Production of Nanofibers

E. García-López, D. Olvera-Trejo, L. F. Velásquez-García
Sponsorship: MIT-Tecnológico de Monterrey Nanotechnology Program

Electrospinning is a versatile process that creates ultrathin nanofibers via electro-hydrodynamical jetting. Electrospun nanofibers are used in a wide variety of biomedical (i.e., tissue healing/scaffolding, drug delivery), energy (i.e., electrodes, solar cells), and microsystem applications (i.e., sensors, batteries). Even though electrospinning is the only technique capable of generating nanofibers of arbitrarily length using a wide variety of feedstock, the throughput of an electrospinning emitter is very low, making difficult the use of these fibers in commercial products. Multiplexing the emitters, i.e., implementing arrays of emitters that work in parallel, is an attractive approach to increase the throughput of electrospinning sources without sacrificing the quality of the fibers generated. Microfabricated multiplexed electrospinning sources that achieve uniform operation at low voltage and large emitter density have been reported. However, these devices do not really solve the problem well as they are made with standard microfabrication, which is expensive and time-consuming.

In this project, we are exploring stereolithography (SLA) to create disposable electrospinning sources capable of high-throughput generation of fibers. In SLA, UV light is focused on a photopolymer while 3-D layers are created through crosslinking, making it possible to print complex three-dimensional structures. The SLA process has several advantages over competing approaches such as a higher resolution, higher quality surface, higher customization, and the creation of watertight imprints.

Devices with emitters with 300-µm internal diameter have been created (Figure 1). Measured per-emitter vs. flow rate characteristics using a PEO solution demonstrates that the arrays operate uniformly. Current research focuses on maximizing the throughput of the sources by emitter multiplexing, exploring approaches for charging up the emitted jets to produce thinner fibers, and in collecting and characterizing aligned PEO nanofibers using a drum as a collector system for tissue engineering applications (Figure 2).

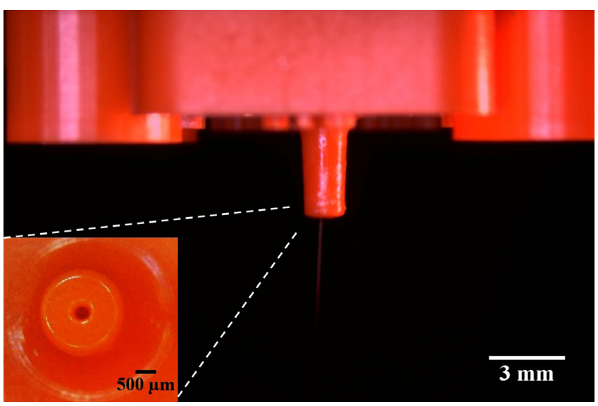

▲ Figure 1: 3-D printed device with one emitter producing PEO nanofibers.

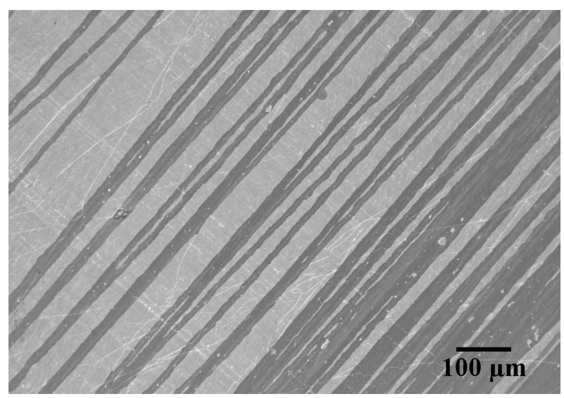

▲ Figure 2: Aligned PEO nanofibers collected using a rotating drum collector.

FURTHER READING

- P. J. Ponce de Leon, F. A. Hill, E. V. Heubel, and L. F. Velásquez- García, "Parallel Nanomanufacturing via Electrohydrodynamic Jetting from Microfabricated Externally Fed- Fed Emitter Arrays," *Nanotechnology*, vol. 26, no. 22, 225301-1-225301-10, 2005.
- L. F. Velásquez- Garcia, "SLA 3-D Printed Arrays of Miniaturized, Internally Fed Polymer Electrospray Emitters," *J. Microelectromechanical Systems*, vol. 24, no. 6, 2117-2127, Dec. 2015.
- D. Olvera-Trejo and L. F. Velásquez-García, "Additively Manufactured MEMS Multiplexed Coaxial Electrospray Sources for High-Throughput, Uniform Generation of Core-Shell Microparticles," *Lab on a Chip*, vol. 16, no. 21, 121 – 4132, Nov. 2016.

Atmospheric Microplasma-Based 3-D Printing of Metallic Microstructures

Y. Kornbluth, R. Mathews, L. Parameswaran, L. M. Racz, L. F. Velásquez-García
Sponsorship: MIT Lincoln Laboratory

State-of-the-art additive manufacturing techniques for metallic microstructures cannot yet deliver the feature resolution, electrical conductivity, and material choice flexibility needed for high-performance microcircuits. Further, many current and proposed additive manufacturing approaches for fine-geometry metal features require high-temperature post-processing and restrict the substrate material. We aim to develop a microplasma-based sputtering system able to direct write a wide range of materials onto any substrate. We have modeled, designed, and constructed a first-generation system that sputters gold onto a substrate. By manipulating the metal at the atomic level, we retain the resistivity of bulk metal, and by sputtering the metal, we eliminate the need for post-processing or lithographic patterning.

We use a microplasma to sputter metal at atmospheric pressure, obviating the need for a vacuum. Our microplasma generator uses electrostatic fields to focus the imprints. With a suitable electrode arrangement, we can shape electrostatic fields that will guide the ionized fraction of the working gas towards a localized spot on the substrate. The directed ions will collide with other gas atoms and, crucially, with sputtered metal atoms from the sputtering target. The net force due to these collisions will indirectly guide the metal atoms towards the desired part of the substrate. This indirect electrostatic focusing not only mitigates the inherent spread of the sputtered material caused by collisions at atmospheric pressure, but also enables feature definition. In the absence of collisions, the printed line will be wider than the sacrificial cathode. By focusing the sputtered material, we achieve imprints significantly narrower than the cathode. This precludes the need to machine sacrificial electrodes as small as our desired printed lines.

Our microplasma head has a central target wire acting as the cathode, surrounded by four electrodes (Figure 1), two biased at a positive voltage (relative to the grounded target) to form the plasma, and the other two biased at a negative voltage to focus the plasma. By both pulling and pushing the plasma, COMSOL simulations predict imprints orders of magnitude narrower than the cross section of the target wire (Figure 2).

▲ Figure 1: A picture of two electrode assemblies. The target wire is installed at the center of the structure. The resulting plasma sputters metal atoms from the target, which then are carried towards the substrate by the gas flow and the electrostatic drag.

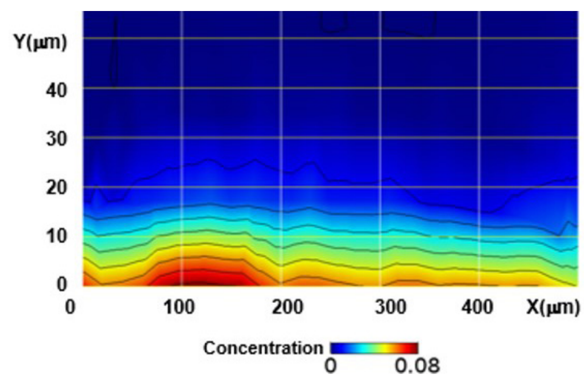

▲ Figure 2: COMSOL simulation results showing a top-down view of the distribution of sputtered material on the substrate. Only one quarter of the substrate is shown because the simulation is symmetric on the two in-plane axes. For an optimized set of parameters, simulations predict that a 15-μm-wide (full width half maximum) gold line is printed on the substrate.

FURTHER READING

- A. M. Abdul-Wahed, A. L. Roy, Z. Xiao, and K. Takahata, "Direct Writing of Thin and Thick Metal Films via Micro Glow Plasma Scanning," *Technical Digest 29th IEEE Conference on Micro Electro Mechanical Systems (MEMS 2016)*, 443-446, Jan., 2016.
- E. D. Burwell IV, "A Microplasma-Based Sputtering System for Direct-Write, Microscale Fabrication of Thin-Film Metal Structures," Master's Thesis, Case Western Reserve University, Cleveland, 2016.

MEMS Electrohydrodynamic High-Throughput Core-Shell Droplet Sources

D. Olvera-Trejo, L. F. Velásquez-García
Sponsorship: MIT-Tecnológico de Monterrey Nanotechnology Program

Coaxial electrospraying is a microencapsulation technology based on electrohydrodynamic jetting of two immiscible liquids that allows precise control with low size variation of the geometry of the core-shell particles it generates. Coaxial electrospraying is a very promising microencapsulation technique because (i) it is easy to implement, (ii) it can operate at room temperature and at atmospheric pressure, (iii) it does not require a series of steps in the encapsulation process, (iv) it can generate compound droplets with narrow size distribution, and (v) it can be used to encapsulate a great variety of materials of interest to biomedical and engineering applications. State-of-the-art coaxial electrospray sources have very low throughput because they have only one emitter. Consequently, coaxial electrosprayed compound particles are compatible with only high-end applications and research.

An approach to increasing the throughput of a coaxial electrospray source without affecting the size variation of the emitted compound microparticles is to implement arrays of coaxial emitters that operate in parallel. However, no miniaturized coaxial array sources have been reported, probably due to the inherent three-dimensionality of the emitter geometry and the hydraulic network required for uniform array operation, which is at odds with the planar nature of traditional microfabrication. In this project, we demonstrated the first MEMS multiplexed coaxial electrospray sources in the literature. Miniaturized core-shell particle generators with up to 25 coaxial electrospray emitters (25 emitters·cm^{-2}) were fabricated via digital light projection/stereolithography (DLP/SLA, Figure 1), which is an additive manufacturing process based on photopolymerization of a resin that can create complex microfluidics. The characterization of emitter arrays with the same emitter structure but different array size demonstrates uniform array operation. The core/shell particles produced by these additively manufactured sources are very uniform (Figure 2); the size distribution of these compound microparticles can be modulated by controlling the flow rates fed to the emitters.

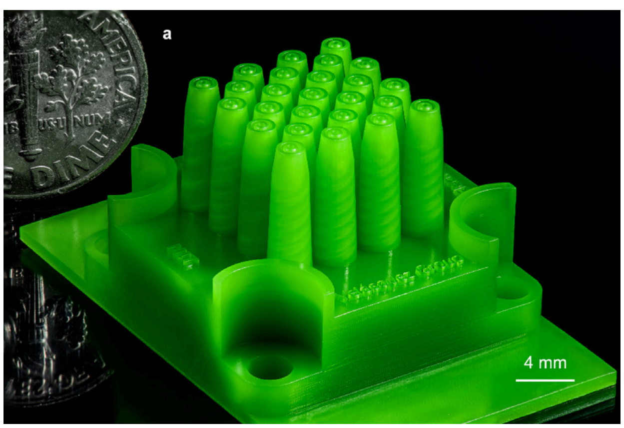

▲ Figure 1: DLP/SLA 3-D printed monolithic array of coaxial electrospinning emitters.

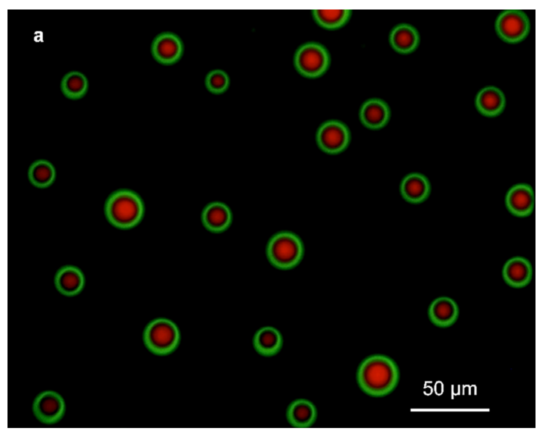

▲ Figure 2: Core-shell microdroplets generated by massively multiplexed MEMS coaxial electrospray sources. The feedstock was colored with fluorescent dyes to help visualize the structure of the droplets.

FURTHER READING

- L. F. Velásquez-García, "SLA 3D-Printed Arrays of Miniaturized, Internally-Fed, Polymer Electrospray Emitters," *J. Microelectromechanical Systems*, vol. 24, no. 6, 2117–2127, 2015.
- D. Olvera-Trejo and L. F. Velásquez-García, "Additively Manufactured MEMS Multiplexed Coaxial Electrospray Sources for High-Throughput, Uniform Generation of Core-Shell Microparticles," *Lab Chip*, vol. 16, no. 21, 4121–4132, 2016.
- A. Taylor and L. F. Velásquez-García, "3D Printed Miniaturized Diaphragm Vacuum Pump," *Technical Digest 30th IEEE Conference on Micro Electro Mechanical Systems (MEMS 2017)*, 1292–1295, Jan. 2017.

High Current Density Si-field Emission Arrays (FEAs)

G. Rughoobur, S. A. Guerrera, A. I. Akinwande
Sponsorship: RAVEN/IARPA

Silicon field emitter arrays (FEAs) are excellent cold cathodes that have not been fully exploited due to the nonzero tip radius distribution causing lower utilization of the arrays. This discrepancy in emitter tips causes sharper tips to burn out (by Joule heating) before duller tips, and therefore the maximum current achievable is small. In this work, we focus on achieving high current density Si FEAs, by integrating high-aspect ratio Si nanowires as to limit the supply of electrons and hence saturate the maximum current to avoid the burn-out of the sharper tips.

Si nanowires of height ~10 µm and 100-200-nm diameter limit the current and improve reliability through velocity saturation and the pinch-off of majority carriers. To prevent charge injection and minimize the gate-substrate capacitance, a 2-µm-thick SiO_2 insulator is added, and the Si nanowires are embedded in a conformal dielectric matrix consisting of Si_3N_4 and SiO_2. High current densities are achieved as the nanowires (current limiter) are integrated with each field emitter, thereby preserving a high density of operational emitters (~10^8 emitters/cm²) without burning out. These Si FEAs have also been shown to provide consistent current scaling of array sizes from a single emitter to 25,000 emitters, low voltage (V_{GE} < 60 V), high current density (J > 100 A/cm²), and long lifetime (τ > 100 hours at 100 A/cm², > 100 hours at 10 A/cm², and > 300 hours at 100 mA/cm²). Compared to conventional Si FEAs operating without a current limiter, the device architecture shown here demonstrate a current density improvement of > 10 folds and low turn-on voltage (8.5 V). Cold cathodes based on Si-FEAs incorporating a current limiter have high potential in applications ranging from X-ray imaging, RF amplifiers, and THz sources to deep UV sources, ion sources, and neutron sources.

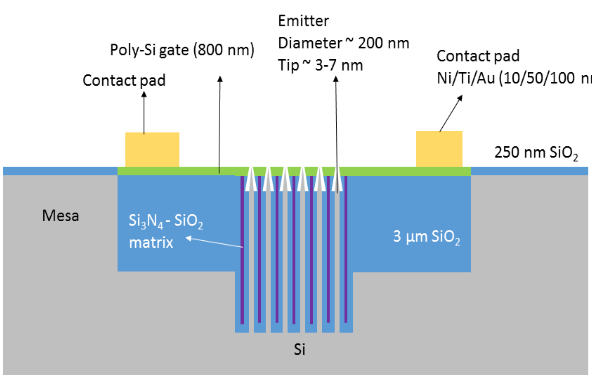

▲Figure 1: Device architecture demonstrating the 200-nm-diameter 10-µm-tall Si nanowires integrated below the field emitters, embedded in a dielectric matrix encapsulated with a poly-Si gate and metal pads for contact.

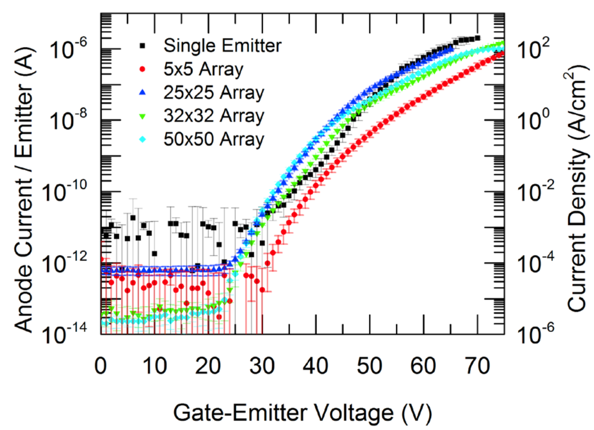

▲Figure 2: Comparison of the transfer characteristics of 5 different devices scaled by the number of emitters showing values of J ~ 100 A/cm².

FURTHER READING

- S. A. Guerrera and A. I. Akinwande, "Nanofabrication of Arrays of Silicon Field Emitters with Vertical Silicon Nanowire Current Limiters and Self-Aligned Gates," *Nanotechnology*, vol. 27, no. 295302, 11, Jun. 2016.
- S. A. Guerrera, L. F. Velasquez-Garcia, and A. I. Akinwande, "Scaling of High-Aspect-Ratio Current Limiters for the Individual Ballasting of Large Arrays of Field Emitters," *IEEE Transactions on Electron Devices*, vol. 59, no. 9, 2524-2530, Sept. 2012.
- S. A. Guerrera and A. I. Akinwande, "Silicon Field Emitter Arrays with Current Densities Exceeding 100 A/cm2 at Gate Voltages Below 75 V," *IEEE Electron Device Lett.*, vol. 37, no. 1, 96-99, Jan. 2016.

Field Emission from Silicon Tips Embedded in a Dielectric Matrix

N. Karaulac, S. A. Guerrera, M. T. Cole, W. I. Milne, A. I. Akinwande
Sponsorship: DARPA, IARPA

Field emitter arrays (FEAs) are a class of cold cathodes with promising potential in a variety of applications requiring high current density electron sources. However, FEAs have not yet achieved widespread usage because of fundamental challenges that limit their reliability in systems. Field emission from conducting surfaces requires high fields and pristine surfaces; these surfaces are vulnerable to adsorption-desorption processes by residual gas molecules, leading to emission current fluctuations and tip erosion. Moreover, electron transport through insulators often leads to impact ionization and dielectric breakdown. This project explores electron emission from field emitter tips that are embedded in a dielectric matrix, specifically silicon dioxide, as a potential approach to address reliability problems in classical field emitters.

In the project, arrays of silicon emitter tips that are individually regulated by silicon nanowires are being fabricated. The silicon nanowires have diameters between 100-200 nm and heights of 10 µm, resulting in an aspect ratio of 50-100:1. The emitter tips typically have radii of 5 nm with a log-normal distribution and a density of 10^8 tips/cm^2. Further, the silicon nanowires function as current limiters that improve reliability by preventing premature tip burn-out due to Joule heating, thermal runaway, and cathodic arcs. Chemical mechanical polishing (CMP) was used to form the self-aligned gates. The silicon tips formed by oxidation sharpening are embedded in a dielectric matrix and are not released. A diagram of the structure is shown in Figure 1.

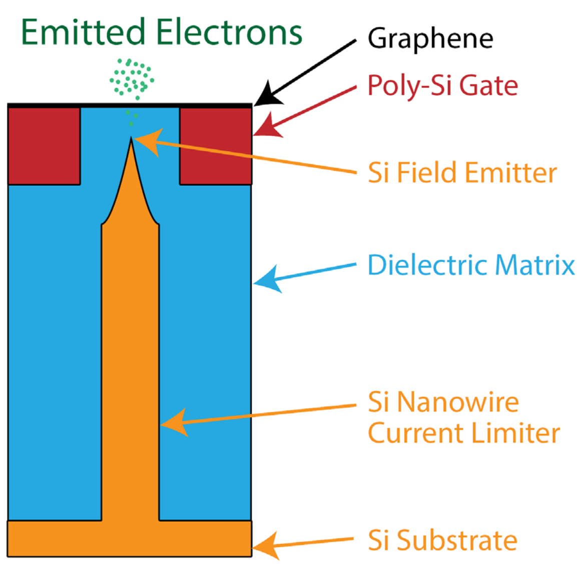

▲Figure 1: Diagram of a silicon field emitter tip embedded in silicon dioxide with single-layer graphene on top.

FURTHER READING

- S. A. Guerrera and A. I. Akinwande, "Nanofabrication of Arrays of Silicon Field Emitters with Vertical Silicon Nanowire Current Limiters and Self-Aligned Gates," *Nanotechnology*, vol. 27, no. 29, 295302:1-11, Jun. 2016.
- C. Li, M. T. Cole, W. Lei, K. Qu, K. Ying, Y. Zhang, A. R. Robertson, J. H. Warner, S. Ding, X. Zhang, B. Wang, and W. I. Milne, "Highly Electron Transparent Graphene for Field Emission Triode Gates," *Advanced Functional Materials*, vol. 24, no. 9, 1218-1227, Mar. 2014.

A Silicon Field Emitter Array as an Electron Source for Phase Controlled Magnetrons

W. Chern, S. Guerrera, A. I. Akinwande
Sponsorship: AFOSR

Magnetrons are a highly efficient (>90%), high-power vacuum-based microwave source. In a magnetron, free-electrons in vacuum are subject to a magnetic field while moving past open metal cavities, resulting in resonant microwave radiation to be emitted. Current state-of-art magnetrons use a heated metal filament to thermionically emit electrons into vacuum continuously and are not addressable. This work seeks to replace the heated metal filament as a source of electrons with silicon field emitter arrays in order to improve the efficiency and increase the power, especially when several sources are combined. Silicon field emitter arrays, schematic shown in Figure 1, are devices that are normally off and are capable of high current densities plus spatial and temporal addressing. These arrays consist of a many sharp tips made of silicon sitting on long silicon nanowires that limit the current of the electron emission. Electrons from the silicon tip tunnel into a vacuum as a result of the high electric field of the applied bias on the polysilicon gate. Pulsing the electric field applied on the gate can turn the arrays on and off. The proposed use of silicon field emitter arrays in a magnetron will allow injection locking and hence phase control of magnetrons. Phase-controlled magnetrons have multiple applications in areas where high-power microwave sources are desired.

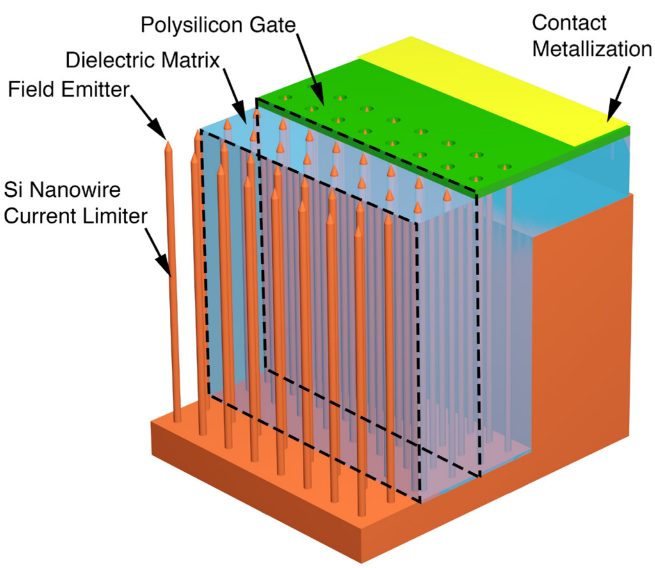

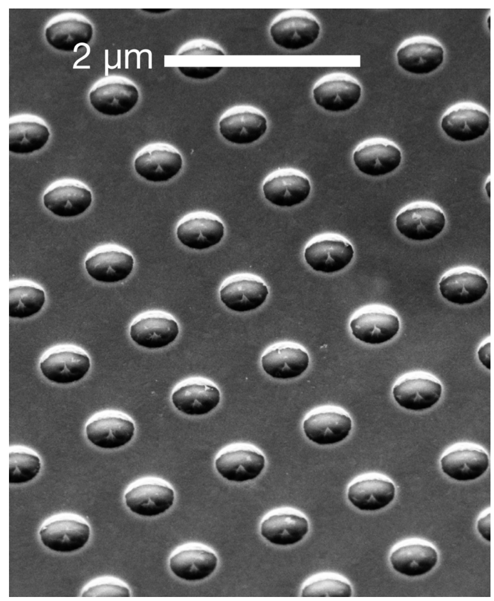

▲ Figure 1: (Left) 3-D rendering of Si device structure. For clarity, layers have been omitted in different regions of the rendering to show detail. In the front, the bare silicon nanowires [200-nm diameter & 10-μm height] with sharp tips. (Right) Top-view of a fabricated device with 350-nm gate aperture and 1-μm tip-to-tip spacing.

FURTHER READING

- S. Guerrera and A. I. Akinwande, "Silicon Field Emitter Arrays with Current Densities Exceeding 100 A/cm² at Gate Voltages Below 75 V," in *Proc. IEDM*, 2016.

Ion Electrospray Thrusters for Microsatellite Propulsion

D. Freeman, D. Krejci, C. Fucetola, H. Li, A. Bost, P. Lozano
Sponsorship: U.S. Department of Defense

Ion electrospray propulsion systems (iEPS) are high specific impulse, low thrust, and extremely scalable devices; these characteristics make them excellent candidates for propulsion systems on microsatellites, which require some small amount of maneuverability primarily for station-keeping. Like other ion engines, they utilize an electrostatic potential to accelerate charged particles across a gap to relatively high velocities to generate thrust. Utilizing ionic liquids – a special class of molten salts that do not evaporate in vacuum, thanks to their negligible vapor pressure – drastically increases the propellant density and obviates the need for a stage in which the propellant is first ionized, thus further reducing mass and volume requirements. The thrusters themselves are extremely simple in that they are passively fed through capillary action and require no moving parts. However, high electric fields, on the order of 10^9 V m^{-1}, are required to extract ions from the liquid. This entails careful fabrication of the porous emitter substrates, which feature an array of roughly five hundred tips, patterned into the surface via laser ablation. By providing a sharp tip, the electric field is effectively intensified to the point that ions can be extracted, through a sharpening effect similar to coronal discharge.

The thrusters are constructed from several component parts. The frames are made via microelectromechanical (MEMS) processing: a silicon base layer, an insulating glass layer, and finally a top silicon layer with alignment features to correctly locate the tip array is etched and then anodically bonded. To those frames a porous substrate is affixed after being shaped and polished. A tip array is patterned into the substrate via laser ablation. Next, a silicon electrode grid, also fabricated with MEMS processing, is bonded to the frame so that the grid holes are aligned to the tip array, completing the emitter. The emitters are then bonded onto tanks that passively transport propellant to the emitter. The tanks are mounted on electronic power supply/control boards, creating a finished engine that may be integrated into a spacecraft. Four small satellites (CubeSats) equipped with these thrusters have already been launched into space. Our team is currently working on a new project, set to launch during Q1 of 2018.

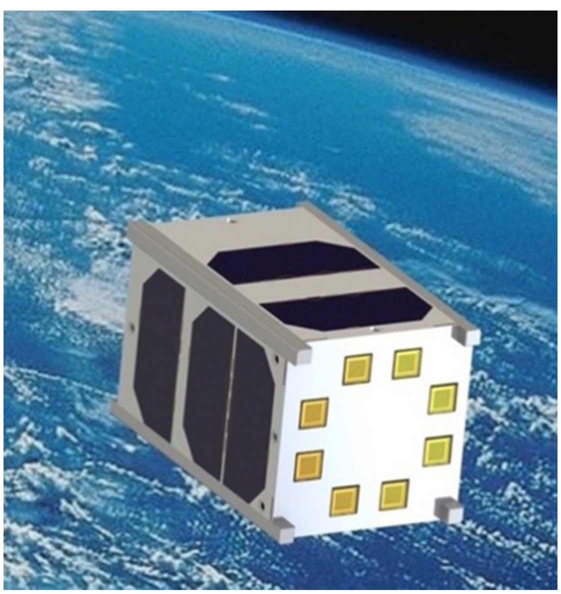

▲Figure 1: Illustration of 8 iEPS emitters, mounted on a small satellite.

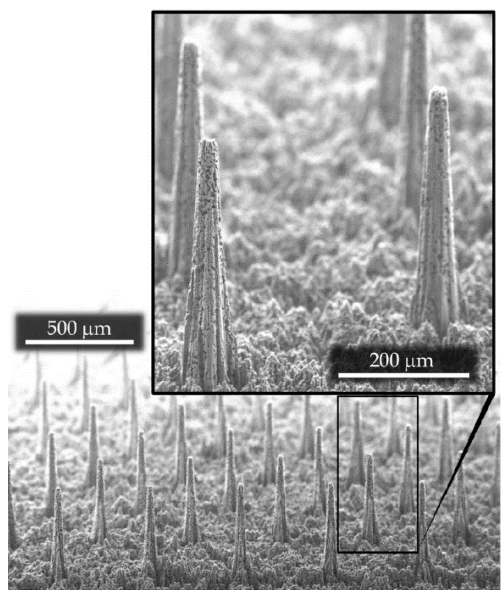

▲Figure 2: SEM of a patterned emitter chip. Periodically blanking the beam of a picosecond 355-nm laser ablates the material around the tips.

Enhanced Water Desalination in Electromembrane Systems

S. Choi, B. Kim, J. Yoon, J. Han, B. Al-Anzi, J. White, S. V. Pham
Sponsorship: Kuwait-MIT Center Signature Research Project, KFAS

Currently, reverse osmosis (RO) is considered the leading technology for desalination, and the operational efficiency of RO has been significantly improved over the last two decades with a thorough energy analysis. On the other hand, electrical desalination can be more advantageous in certain applications due to the diversity of allowed feed conditions, operational flexibility, and the relatively low capital cost needed (the size of a system is generally small). Yet, electromembrane desalination techniques such as electrodialysis (ED) have not been modeled in full detail, partially due to scientific challenges involving the multiphysics nature of the process.

In addition, while current ED relies on bipolar ion conduction (Figure 1b), removing one pair of a cation and an anion simultaneously, one final but most important point is that desalination achieved by means of an anion exchange membrane (AEM) and a cation exchange membrane (CEM) should be considered separately and independently (Figure 1a). Based on the intrinsically different ion transport near AEM and CEM, our group previously presented a novel process of ion concentration polarization (ICP) desalination (Figure 1b), which can basically enhance the amount of salt reduction, by examining unipolar ion conduction through both experiments and numerical modeling. In our studies, we investigate the effects of embedded microstructures on mass transport enhancement; these microstructures affect the electrical energy efficiency of an ED system for its current application of brackish (low salinity) water desalination (Figure 1c); we also explore the technical and economic feasibility of the ICP desalination for potential applications in the emerging field of high-salinity brine desalination (Figure 1d).

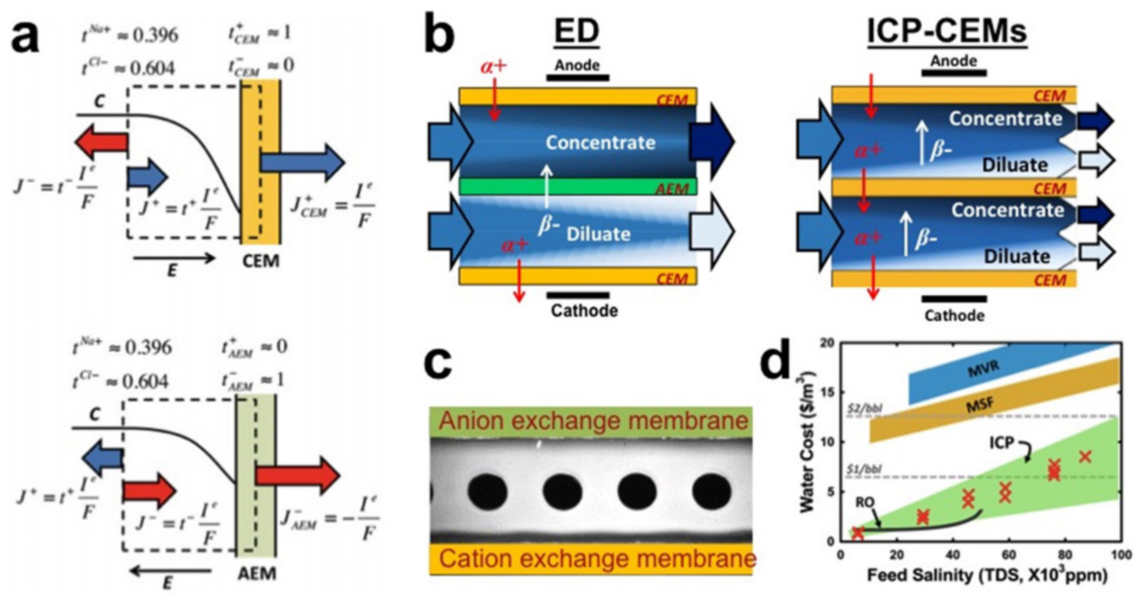

▲ Figure 1: (a) Schematic diagram of counter-ion/co-ion transport near CEM/AEM, (b) schematics of ED (left) and ICP desalination (right), (c) microfluidic image of ED channel with embedded structures, (d) water cost plot for various desalination technologies in a range of feed salinities.

FURTHER READING

- R. Kwak, V. S. Pham, B. Kim, L. Chen, and J. Han, "Enhanced Salt Removal by Unipolar Ion Conduction in Ion Concentration Polarization Desalination," *Scientific Reports*, vol. 6, 25349, 2016.
- B. Kim, S. Choi, S. V. Pham, R. Kwak, and J. Han, "Energy Efficiency Enhancement of Electromembrane Desalination Systems by Local Flow Redistribution Optimized for the Asymmetry of Cation/Anion Diffusivity," *J. Membrane Science*, doi:10.1016/j.memsci.2016.11.046, 2016.
- B. Kim, R. Kwak, H. J. Kwon, V. S. Pham, M. Kim, B. Al-Anzi, G. Lim, and J. Han, "Purification of High Salinity Brine by Multi-Stage Ion Concentration Polarization Desalination," *Scientific Reports*, vol. 6, 31850, 2016.